Modelling heat and mass transfer of a CO_2 binary mixture: a mathematical approach

R.O. Olayiwola[*†], A.T. Cole[*], M.D. Shehu[*], F.A. Oguntolu[*], E.E. Iyeme[‡], and A.W. Abubakar[§]

Abstract

This paper presents an analytical solutions for describing heat and mass transfer between a droplet of organic solvent and a compressed antisolvent taking into consideration the viscous energy dissipation and heat and mass transfer between the surface and the droplet by convection. The solvent and antisolvent are assumed to be fully miscible and have the same temperature. Both the initial temperature of the mixture and the initial carbon dioxide concentration are also assumed to depend on the space variable. The governing equations formulated based on the conservation of total mass, chemical species, momentum and energy were solved analytically using polynomial approximation method. The results obtained are presented graphically and discussed. The results revealed the effects of operating parameters on droplet lifetime. These results might be used for interpretation or experiments planning of the more complex real supercritical antisolvent process.

Keywords: carbon dioxide; drug particles; polynomial approximation method; precipitation; solvent; supercritical fluid.

1 Introduction

Particle formation technologies are important in the pharmaceutical industries, and in the production of photographic materials, ceramics, explosives, and dyes. The focus in drug formulation is to develop techniques that give more consistent and controlled particle size, morphology, and uniformity [4]. In current drug delivery technology, very small drug particles are of interest since they can travel faster to the target organ and distribute more evenly in the body [7].

Conventional methods for manipulating pharmaceutical particles include jet milling, spray drying, and emulsion techniques [2]. Jet milling uses particle-to-particle impact forces to break up the products into smaller pieces [10]. However, the jet milling process generally does not produce a uniform particle size distribution and running the process consumes a lot of energy [2]. Freeze drying results in particles of broad size ranges and usually require subsequent milling and sieving [12]. Spray drying usually gives

[*]Department of Mathematics, Federal University of Technology, Minna, Nigeria
[†] Corresponding Author. E-mail: olayiwola.rasaq@futminna.edu.ng
[‡]Department of Mathematics, Cross River University of Technology, Calabar, Nigeria
[§]Department of Mathematics, Air Force Institute of Technology, Kaduna, Nigeria

R.O. Olayiwola, A.T. Cole, M.D. Shehu, F.A. Oguntolu, E.E. Iyeme, and A.W. Abubakar

particles of controllable size, but the extreme temperatures used during the operation can denature biological materials [17].

Conventional drug particle precipitation uses organic solvents as antisolvents for precipitation or as emulsifiers for emulsion process [18]. Traces of residual organic solvents, such as methylene chloride, that may still be in the drug particles have motivated researchers to find alternative methods for particle formation [16]. An alternative to reduce this problem is to use supercritical carbon dioxide (CO_2) as an antisolvent to precipitate drug particles from solution since CO_2 is nonflammable, non-toxic, inexpensive, renewable, and environmentally benign [11].

A supercritical fluid is any substance at a temperature and pressure above its critical point, where distinct liquid and gas phases do not exist. It can effuse through solids like a gas, and dissolve materials like a liquid. Carbon dioxide and water are the most commonly used supercritical fluids [14].

In order to successfully design a CO_2 antisolvent process, it is important to understand the effects of the operating parameters on particle characteristics. However, Bristow *et al.* [3] explained experimental particle size and morphology results in light of current hydrodynamic, kinetic and thermodynamic theories.

In the face of experimental difficulties, mathematical modeling appears as a useful tool to determine important parameters of the process. In view of this, Kumar *et al.* [9] developed a mathematical model of the droplet moving in a supercritical carbon dioxide environment. The solvent chosen in their study is ethanol. They solved the equations using MATLAB software. Chong *et al.* [5] presented a numerical procedure of mathematical model for mass transfer between a droplet of organic solvent and a compressed antisolvent which is applicable to the supercritical antisolvent (SAS) method of particle formation. Their model equations were put into the form that allowed the application of the MATLAB standard solver pdepe. Wu *et al.* [19] modelled the mixing of a hydrocarbon droplet, containing a mixture of toluene and either n-decane or tetralin, in a reservoir of supercritical or near-critical water. Their study provided microscale information, such as multi-component partitioning, and insight into large scale mixing in applications. Almeida *et al.* [1] used a three-dimensional mathematical model to study the development of a jet of solution (ethanol and minocycline) expanded in pressurized carbon dioxide in order to interpret the process of development of regions of supersaturation of the solution. The commercial code ANSYS FLUENT was used to solve the model relating the impact of the flow of solution in the mixing chamber of the precipitation process.

In this paper, a mathematical model capable of predicting the composition of hydrocarbon and carbon dioxide in SAS process is presented. We assume constant density, diffusivity and thermal conductivity. The droplet is moving through CO_2 continuum and heat and mass transfer take place to and from the droplet which led to the supersaturation and then fine particle of solute. To simulate the flow analytically, we assume that the medium is not stagnant so the convective flux can be considered.

2 Model formulation

A 'pseudo' droplet of solvent (hydrocarbon droplet) immersed in a compressed antisolvent (carbon dioxide) in miscible conditions is considered. The space variable is r, $0 \le r \le R$, and time is t, $t > 0$ The state variables depending on (r, t) are the mixture temperature T, carbon dioxide mole fraction

X_c, solvent mole fraction X_h, radial velocity of droplet u and pressure p. The formulation of our model is guided by the following assumptions:

1. The solvent and the antisolvent are fully miscible so only one equation is needed to describe the mass transfer.
2. The medium is not stagnant so the convective flux can be considered.
3. The radial velocity (velocity of droplet) is non-zero because of temperature change and mixing of carbon dioxide and hydrocarbons.
4. The heat and mass transfer between the surface and the mixture take place by convection.
5. The spherical symmetry is considered, making the problem one-dimensional.
6. The viscous energy dissipation is considered.
7. There is no heat source.

The diffusive flux is assumed to be proportional to the concentration gradient as described by Fick's law:

$$N_c = -\rho D \nabla X_c + X_c N. \tag{1}$$

The mass balance on carbon dioxide reads:

$$\frac{\partial}{\partial t}(\rho X_c) + \nabla \cdot (-\rho D \nabla X_c + X_c N) = 0. \tag{2}$$

The continuity equation required to find the convective flux N is:

$$\frac{\partial \rho}{\partial t} + \nabla \cdot N = 0. \tag{3}$$

Multiplying (3) by X_c and combining with (2) yields:

$$\rho \frac{\partial X_c}{\partial t} + N\nabla \cdot X_c = \nabla \cdot (\rho D \nabla X_c). \tag{4}$$

In a similar manner, momentum and energy conservation equations can be obtained respectively as:

$$\rho \frac{\partial u}{\partial t} + N\nabla \cdot u = -\frac{\partial p}{\partial x} + \frac{\partial}{\partial x}\left(2\mu \frac{\partial u}{\partial x} - \frac{2}{3}\mu \nabla \cdot u\right) \tag{5}$$

$$c_p\left(\rho \frac{\partial T}{\partial t} + N\nabla \cdot T\right) = \nabla \cdot (\lambda \nabla T) + \rho c_p D \frac{1000}{M} \frac{\partial X_c}{\partial x} \frac{\partial T}{\partial x} + \mu\left(2\left(\frac{\partial u}{\partial x}\right)^2 - \frac{2}{3}\left(\frac{\partial u}{\partial x}\right)^2\right). \tag{6}$$

Introducing an apparent flux to replace convective flux (i.e., $N = \rho u$) yields in one-dimensional Cartesian coordinates:

$$\frac{\partial \rho}{\partial t} + \frac{\partial}{\partial x}(\rho u) = 0 \tag{7}$$

$$\rho\left(\frac{\partial u}{\partial t}+u\frac{\partial u}{\partial x}\right)=-\frac{\partial p}{\partial x}+\frac{\partial}{\partial x}\left(2\mu\frac{\partial u}{\partial x}-\frac{2}{3}\mu\frac{\partial u}{\partial x}\right),\tag{8}$$

$$\rho\left(\frac{\partial X_c}{\partial t}+u\frac{\partial X_c}{\partial r}\right)=\frac{\partial}{\partial x}\left(\rho D\frac{\partial X_c}{\partial x}\right),\tag{9}$$

$$\rho c_p\left(\frac{\partial T}{\partial t}+u\frac{\partial T}{\partial x}\right)=\frac{\partial}{\partial x}\left(\lambda\frac{\partial T}{\partial x}\right)+\rho c_p D\frac{1000}{M}\frac{\partial X_c}{\partial x}\frac{\partial T}{\partial x}+\mu\left(2\left(\frac{\partial u}{\partial x}\right)^2-\frac{2}{3}\left(\frac{\partial u}{\partial x}\right)^2\right).\tag{10}$$

We can eliminate the continuity equation (7) by means of streamline function (see, [13]),

$$\eta(x,t)=\left(\rho^2\right)^{\frac{1}{2}}\int_0^x\rho(s,t)ds\tag{11}$$

The coordinate transformation becomes,

$$\frac{\partial}{\partial x}\rightarrow\frac{\partial}{\partial\eta}\frac{\partial\eta}{\partial x}=\frac{\partial}{\partial\eta}\tag{12}$$

$$\frac{\partial}{\partial t}\rightarrow\frac{\partial}{\partial\eta}\frac{\partial\eta}{\partial t}+\frac{\partial}{\partial t}=-u\frac{\partial}{\partial\eta}+\frac{\partial}{\partial t}.\tag{13}$$

We make the additional assumptions that c_p, λ, μ and ρD are constant. Although these assumptions could be relaxed in the future, they considerably simplify the equations. The equations can be simplified as

$$\frac{\partial u}{\partial t}=-\frac{1}{\rho}\frac{\partial p}{\partial\eta}+\upsilon\frac{\partial}{\partial\eta}\left(2\frac{\partial u}{\partial\eta}-\frac{2}{3}\frac{\partial u}{\partial\eta}\right)\tag{14}$$

$$\frac{\partial X_c}{\partial t}=D\frac{\partial}{\partial\eta}\left(\frac{\partial X_c}{\partial\eta}\right)\tag{15}$$

$$\frac{\partial T}{\partial t}=\frac{\lambda}{\rho c_p}\frac{\partial}{\partial\eta}\left(\frac{\partial T}{\partial\eta}\right)+\frac{1000D}{M}\frac{\partial X_c}{\partial\eta}\frac{\partial T}{\partial\eta}+\frac{\upsilon}{c_p}\left(2\left(\frac{\partial u}{\partial\eta}\right)^2-\frac{2}{3}\left(\frac{\partial u}{\partial\eta}\right)^2\right).\tag{16}$$

In spherical coordinates system (see, [6]), (14) – (16) become

$$\frac{\partial u}{\partial t}=-\frac{1}{\rho}\frac{\partial p}{\partial r}+\upsilon\frac{\partial}{\partial r}\left(2\frac{\partial u}{\partial r}-\frac{2}{3}\frac{1}{r^2}\frac{\partial}{\partial r}\left(r^2u\right)\right)\tag{17}$$

$$\frac{\partial X_c}{\partial t}=\frac{D}{r^2}\frac{\partial}{\partial r}\left(r^2\frac{\partial X_c}{\partial r}\right)\tag{18}$$

$$\frac{\partial T}{\partial t}=\frac{\lambda}{\rho c_p r^2}\frac{\partial}{\partial r}\left(r^2\frac{\partial T}{\partial r}\right)+\frac{1000D}{M}\frac{\partial X_c}{\partial r}\frac{\partial T}{\partial r}+\frac{\upsilon}{c_p}\left(2\left(\frac{\partial u}{\partial r}\right)^2+4\left(\frac{u}{r}\right)^2-\frac{2}{3}\left(\frac{\partial u}{\partial r}+\frac{2u}{r}\right)^2\right),\tag{19}$$

where u is the radial velocity (velocity of droplet).

The mole fraction of the solvent (hydrocarbon droplet) is directly deduced by the relation:

$$X_s = 1 - X_c \tag{20}$$

Darcy's law

$$u = -\frac{K}{\mu}\frac{\partial p}{\partial r} \tag{21}$$

To avoid potential convergence problems, the initial and boundary conditions is formulated as follows:

Initial conditions

At $t = 0$ and $\forall r$,

$$u = U_{s}, \quad T = \frac{1}{2}T_{s0}\left(1 + \tanh(a(r - R))\right), \quad X_c = \frac{1}{2}X_{c0}\left(1 + \tanh(a(r - R))\right) \tag{22}$$

Boundary conditions

$$
\left.
\begin{array}{ll}
\left.\dfrac{\partial u}{\partial r}\right|_{r=0} = 0, & \left.\dfrac{\partial u}{\partial r}\right|_{r=R} = q \\[2mm]
\left.\dfrac{\partial X_c}{\partial r}\right|_{r=0} = 0, & D'\left.\dfrac{\partial X_c}{\partial r}\right|_{r=R} = k_m X_c \big|_{r=R} \\[2mm]
\left.\dfrac{\partial T}{\partial r}\right|_{r=0} = 0, & \lambda'\left.\dfrac{\partial T}{\partial r}\right|_{r=R} = hT\big|_{r=R}, \quad T_{c0} > T_{s0} \\[2mm]
p\big|_{r=R} = p_{out}
\end{array}
\right\} \tag{23}
$$

where X_c is the mole fraction of the carbon dioxide, X_s is the mole fraction of the solvent (hydrocarbon droplet), D is the diffusion coefficient of the solvent in the carbon dioxide, ρ is the density of the binary mixture, λ is heat conductivity of the mixture, K is the permeability, R is the droplet radius, T is the temperature of the mixture, M is the molecular weight, T_{c0} is the initial temperature of carbon dioxide, T_{s0} is the initial temperature of hydrocarbon, X_{c0} is the initial concentration of carbon dioxide, T_{s0} is the initial concentration of hydrocarbon, p is the pressure, u is the radial velocity of droplet, U_s is the surface velocity, μ is the dynamic viscosity, c_p is the constant pressure specific heat, r is the radial coordinate, K is the permeability, D' is the effective diffusion coefficient, λ' is the effective heat conductivity, k_m is the convective mass transfer coefficient, h is the convective heat transfer coefficient, p_{out} is the outlet pressure, q is constant.

3   Method of solution
3.1 Dimensional analysis

Dimensionless variables for space and time is been introduced as:

$$r' = \frac{r}{R}, \qquad t' = \frac{t}{t^*}, \qquad t^* = \frac{R}{U_s} \tag{24}$$

Dimensionless variables for radial velocity of droplet, mixture temperature, carbon dioxide mole fraction and hydrocarbon mole fraction is been introduced as follows:

$$\theta = \frac{T}{T_{c0}}, \qquad \phi = \frac{X_c}{X_{c0}}, \qquad \psi = \frac{X_h}{X_{c0}}, \qquad u' = \frac{u}{U_s}, \qquad p' = \frac{p}{\rho U_s^2} \tag{25}$$

where t^* is reference values for time.

Using (24) and (25), and after dropping the prime, equations (17) - (23) become

$$\frac{\partial u}{\partial t} = -\frac{\partial p}{\partial r} + \frac{4}{3}\frac{1}{R_e}\left(\frac{\partial^2 u}{\partial r^2} - \frac{1}{r}\left(\frac{\partial u}{\partial r} - \frac{u}{r}\right)\right) \tag{26}$$

$$\frac{\partial \phi}{\partial t} = \frac{1}{P_{em}}\frac{1}{r^2}\frac{\partial}{\partial r}\left(r^2 \frac{\partial \phi}{\partial r}\right) \tag{27}$$

$$\frac{\partial \theta}{\partial t} = \frac{1}{P_e}\frac{1}{r^2}\frac{\partial}{\partial r}\left(r^2 \frac{\partial \theta}{\partial r}\right) + \frac{\beta}{P_{em}}\frac{\partial \phi}{\partial r}\frac{\partial \theta}{\partial r} + \frac{4}{3}g\frac{E_c}{R_e}\left(\frac{\partial u}{\partial r} - \frac{u}{r}\right)^2 \tag{28}$$

$$\psi(r,t) = \sigma - \phi(r,t) \tag{29}$$

$$\frac{\partial p}{\partial r} = -\frac{1}{D_a R_e}u \tag{30}$$

$$\left.\begin{array}{l} u(r,0) = 1, \qquad\qquad u_r(0,t) = 0, \qquad\qquad u_r(1,t) = \gamma \\[2mm] \phi(r,0) = \frac{1}{2}\left(1 + \tanh\left(\alpha'(r-1)\right)\right), \quad \phi_r(0,t) = 0, \quad \phi_r(1,t) = -Sh\phi(1,t) \\[2mm] \theta(r,0) = \frac{1}{2}\left(1 + \tanh\left(\alpha'(r-1)\right)\right), \quad \theta_r(0,t) = 0, \quad \theta_r(1,t) = -Nu\theta(1,t) \\[2mm] p_r(1,t) = \delta \end{array}\right\} \tag{31}$$

where

$R_e = \frac{RU_s}{\upsilon}$ is the Reynolds number, $P_{em} = \frac{RU_s}{D}$ is the Peclet mass number, $P_e = \frac{\rho c_p RU_s}{\lambda}$ is the

Peclet energy number, $E_c = \frac{U_s^2}{gc_p T_0}$ is the Eckert number, $\sigma = \frac{1}{X_0}$, $\beta = \frac{1000 X_0}{M}$, $\alpha' = \alpha R$,

$D_a = \frac{K}{R^2}$ is the Darcy number, $Sh = \frac{hh}{D}\phi$ is the Sherwood number, $Nu = \frac{hh}{\lambda}$ is the Nusselt number, $\gamma = \frac{Rg}{U_s}$, $\delta = \frac{P_m}{\rho d U_s^2}$

3.2 Solution via Polynomial Approximation Method

Here, we assume polynomial solution of the form (see, [15]):

$$\phi(r,t) = a_0(t) + a_1(t)r + a_2(t)r^2 \tag{32}$$

$$u(r,t) = b_0(t) + b_1(t)r + b_2(t)r^2 \tag{33}$$

$$\theta(r,t) = c_0(t) + c_1(t)r + c_2(t)r^2 \tag{34}$$

Applying the boundary conditions as given in (31), we obtain

$$a_1(t) = b_1(t) = c_1(t) = 0, \quad a_2(t) = -\frac{Sh}{2}\phi|_{r=1}, \quad b_2(t) = \frac{\gamma}{2}, \quad c_2(t) = -\frac{Nu}{2}\theta|_{r=1},$$

$$a_0(t) = \left(1 + \frac{Sh}{2}\right)\phi|_{r=1}, \quad b_0(t) = u|_{r=1} - \frac{\gamma}{2}, \quad c_0(t) = \left(1 + \frac{Nu}{2}\right)\theta|_{r=1} \tag{35}$$

Then, equation (32) – (33) become

$$\phi(r,t) = \left(1 + \frac{Sh}{2}\right)\phi|_{r=1} - \frac{Sh}{2}\phi|_{r=1}r^2 \tag{36}$$

$$u(r,t) = u|_{r=1} - \frac{\gamma}{2} + \frac{\gamma}{2}r^2 \tag{37}$$

$$\theta(r,t) = \left(1 + \frac{Nu}{2}\right)\theta|_{r=1} - \frac{Nu}{2}\theta|_{r=1}r^2 \tag{38}$$

For long spherical shape (see, [8]), we have

$$\bar{\phi} = 3\int_0^1 r^2\phi\,dr \tag{39}$$

$$\bar{u} = 3\int_0^1 r^2 u\,dr \tag{40}$$

$$\bar{\theta} = 3\int_0^1 r^2\theta\,dr \tag{41}$$

where $\bar{\phi}$ is the average mole fraction, $\bar{u}$ is the average velocity, $\bar{\theta}$ is the average temperature. Equations (39) – (41) give the relations

$$\bar{\phi} = \left(1 + \frac{Sh}{2}\right)\phi|_{r=1}, \quad \bar{u} = u|_{r=1} - \frac{2\gamma}{5}, \quad \bar{\theta} = \left(1 + \frac{Nu}{2}\right)\theta|_{r=1} \tag{42}$$

and

$$\frac{\partial}{\partial t}\bar{\phi} = \left(1 + \frac{Sh}{2}\right)\frac{\partial}{\partial t}\phi\Big|_{r=1}, \quad \frac{\partial}{\partial t}\bar{u} = \frac{\partial}{\partial t}u\Big|_{r=1}, \quad \frac{\partial}{\partial t}\bar{\theta} = \left(1 + \frac{Nu}{2}\right)\frac{\partial}{\partial t}\theta\Big|_{r=1} \tag{43}$$

Integrating (26) – (28) with respect to r, yield the following equations

$$\frac{\partial}{\partial t}\phi\bigg|_{r=1} + a\phi\big|_{r=1} = 0 \tag{44}$$

$$\frac{\partial}{\partial t}u\bigg|_{r=1} - bu\big|_{r=1} = c \tag{45}$$

$$\frac{\partial}{\partial t}\theta\bigg|_{r=1} + \left(A - Be^{-at}\right)\theta\big|_{r=1} = D\left(F - Ge^{bt} + E^2 e^{2bt}\right) \tag{46}$$

Solving (44) – (46) gives

$$\phi\big|_{r=1} = \frac{1}{2}e^{-at} \tag{47}$$

$$u\big|_{r=1} = \left(\left(\frac{c}{b}+1\right)e^{bt} - \frac{c}{b}\right) \tag{48}$$

$$\theta\big|_{r=1} = \left(\begin{array}{l} FD\left(\begin{array}{l}\dfrac{1}{A}\left(1-e^{-\left(At+\frac{B}{a}e^{-at}\right)}\right)- \\[2mm] \dfrac{B}{A}\left(\left(e^{-\left(At+\frac{B}{a}e^{-at}\right)}-e^{(1-A)t}\right)+\dfrac{B\sqrt{\pi}}{\sqrt{-aB}}e^{-\left(At+\frac{B}{a}e^{-at}\right)}erf\left(\dfrac{\sqrt{-aB}}{a}\left(e^{-t}-1\right)\right)\right)\end{array}\right)- \\[6mm] DG\left(\begin{array}{l}\dfrac{1}{A+b}\left(e^{bt}-e^{-\left(At+\frac{B}{a}e^{-at}\right)}\right)- \\[2mm] \dfrac{B}{A+b}\left(\left(e^{-\left(At+\frac{B}{a}e^{-at}\right)}-e^{(1-A)t}\right)+\dfrac{B\sqrt{\pi}}{\sqrt{-aB}}e^{-\left(At+\frac{B}{a}e^{-at}\right)}erf\left(\dfrac{\sqrt{-aB}}{a}\left(e^{-t}-1\right)\right)\right)\end{array}\right)+ \\[6mm] DE^2\left(\begin{array}{l}\dfrac{1}{A+2b}\left(e^{2bt}-e^{-\left(At+\frac{B}{a}e^{-at}\right)}\right)- \\[2mm] \dfrac{B}{A+2b}\left(\left(e^{-\left(At+\frac{B}{a}e^{-at}\right)}-e^{(1-A)t}\right)+\dfrac{B\sqrt{\pi}}{\sqrt{-aB}}e^{-\left(At+\frac{B}{a}e^{-at}\right)}erf\left(\dfrac{\sqrt{-aB}}{a}\left(e^{-t}-1\right)\right)\right)\end{array}\right) \\[6mm] + h(1)e^{-\left(At+\frac{B}{a}e^{-at}\right)}\end{array}\right) \tag{49}$$

Substituting equations (47) – (49) into equations (36) – (38) give

$$\phi(r,t) = \frac{1}{2}\left(1+\frac{Sh}{2}\right)e^{-at} - \frac{Sh}{4}r^2 e^{-at} \tag{50}$$

$$u(r,t) = \left(\left(\frac{c}{b}+1\right)e^{bt} - \frac{c}{b}\right) - \frac{\gamma}{2} + \frac{\gamma}{2}r^2 \tag{51}$$

$$\theta(r,t) = \left(1 + \frac{Nu}{2}\right)\theta\Big|_{r=1} - \frac{Nu}{2}\theta\Big|_{r=1}r^2 \tag{52}$$

$$\psi(r,t) = \sigma - \frac{1}{2}\left(1 + \frac{Sh}{2}\right)e^{-at} + \frac{Sh}{4}r^2 e^{-at} \tag{53}$$

$$p(r,t) = \delta + \frac{1}{DaR_e}\left(\left(\left(\frac{c}{b}+1\right)e^{bt} - \frac{c}{b}\right) - \frac{\gamma}{3}\right) - \frac{1}{DaR_e}\left(\left(\left(\frac{c}{b}+1\right)e^{bt} - \frac{c}{b}\right) - \frac{\gamma}{2} + \frac{\gamma}{6}r^2\right)r, \tag{54}$$

where

$$a = \frac{3Sh}{\left(1 + \frac{Sh}{5}\right)P_{em}}, \qquad b = \frac{1}{R_e}\left(4 + \frac{1}{Da}\right), \qquad c = -\frac{1}{R_e}\left(\frac{4}{3} + \frac{1}{5Da}\right),$$

$$A = \frac{Nu}{\left(1 + \frac{Nu}{5}\right)P_e}, \qquad B = \frac{\beta NuSh}{10\left(1 + \frac{Nu}{5}\right)P_{em}}, \qquad D = \frac{4gEc}{3\left(1 + \frac{Nu}{5}\right)R_e},$$

$$E = \left(\frac{c}{b}+1\right), \qquad F = \left(\frac{4\gamma c}{3b} + \frac{4\gamma^2}{9}\right), \qquad G = E\left(\frac{4\gamma}{3} + \frac{2c}{b}\right),$$

$$h(1) = e^{\frac{B}{a}}\left(\frac{1}{2} - \left(\begin{array}{l} FD\left(\frac{1}{A}\left(1 - e^{-\frac{B}{a}}\right) - \frac{B}{A}\left(e^{\frac{B}{a}} - 1\right)\right) - DG\left(\frac{1}{A+b}\left(1 - e^{-\frac{B}{a}}\right) - \frac{B}{A+b}\left(e^{\frac{B}{a}} - 1\right)\right) + \\ DE^2\left(\frac{1}{A+2b}\left(1 - e^{-\frac{B}{a}}\right) - \frac{B}{A+2b}\left(e^{\frac{B}{a}} - 1\right)\right) \end{array}\right)\right)$$

The computations were done on equations (50) – (54) using computer symbolic algebraic package MAPLE 2021.

R.O. Olayiwola, A.T. Cole, M.D. Shehu, F.A. Oguntolu, E.E. Iyeme, and
A.W. Abubakar

4 Results and Discussion

4.1 Analysis of Results

The transport and mixing processes are simulated analytically for a droplet of solvent (hydrocarbon) and a compressed antisolvent (carbon dioxide) in miscible conditions using polynomial approximation method. Analytical solutions given by equations (50) - (54) are computed using computer symbolic algebraic package MAPLE 2021. The numerical results obtained from the method are shown in Figures 1 to 18.

4.2 State Variables Dynamics

We performed the numerical simulations of the system of differential equations of the state variables to determine the changes in the various state variables with time and space. There seems to be a continuous increase in the mixture temperature, droplet velocity, hydrocarbon concentration and pressure as the carbon dioxide concentration decreases with time. Our findings showed an inverse relationship among the mixture temperature, droplet velocity, hydrocarbon concentration, pressure and carbon dioxide concentration as shown in Figures $1 - 5$.

Figure 1 depicts the graph of mixture temperature $\theta(r,t)$ against time t for different values of droplet radius r. It is observed that the temperature of the mixture increases with time and this mixture temperature is higher at the centre of the droplet than at the end of the domain.

Figure 2 shows the graph of carbon dioxide concentration $\phi(r,t)$ against time t for different values of droplet radius r. It is observed that the concentration of carbon dioxide decreases with time and this concentration is higher at the centre of the droplet than at the end of the domain.

Figure 3 displays the graph of hydrocarbon concentration $\psi(r,t)$ against time t for different values of droplet radius r. It is observed that the concentration of hydrocarbon increases with time and this concentration is higher at the end of the domain than at the centre of the droplet.

Figure 4 manifests the graph of droplet velocity $u(r,t)$ against time t for different values of droplet radius r. It is observed that the velocity of droplet increases with time and this velocity is higher at the end of the domain than at the centre of the droplet.

Figure 5 depicts the graph of pressure $p(r,t)$ against time t for different values of droplet radius r. It is observed that the pressure increases with time and this pressure increase throughout the domain except at the end of the domain where it constant.
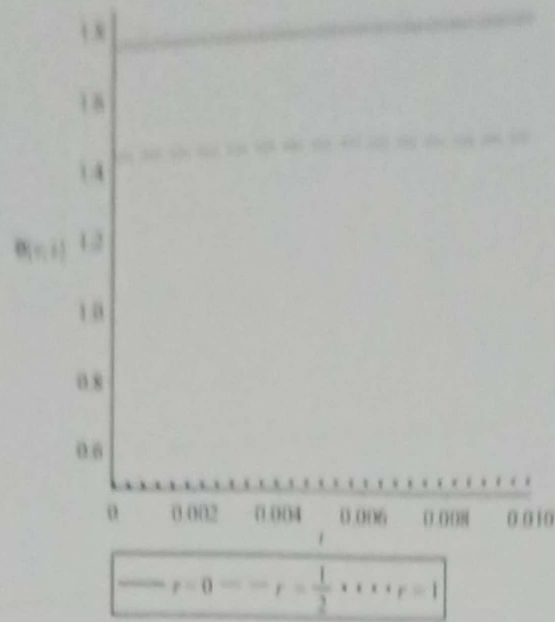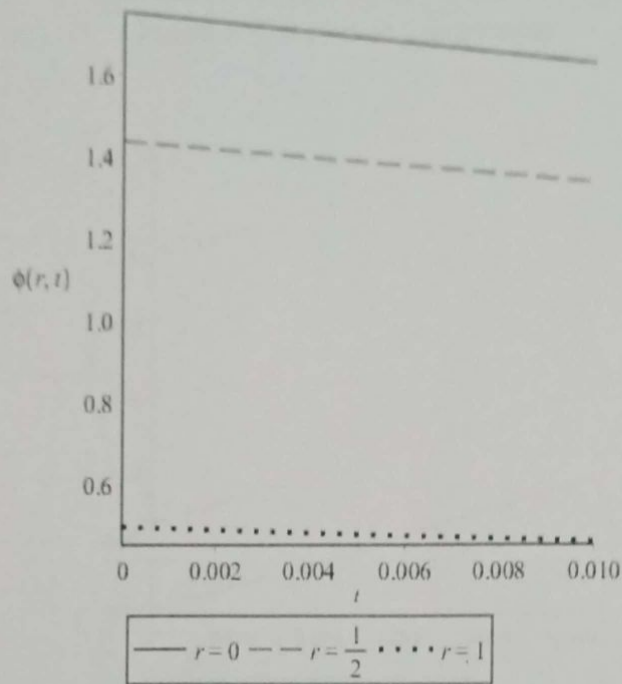
Figure 1: Mixture Temperature

Figure 2: Carbon dioxide Concentration

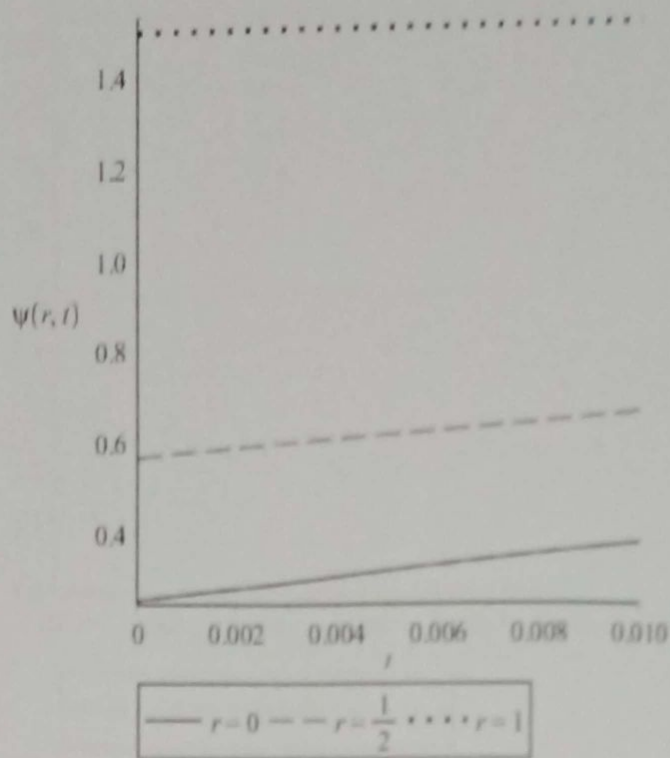R.O. Olayiwola, A.T. Cole, M.D. Shehu, F.A. Oguntolu, E.E. Iyeme, and
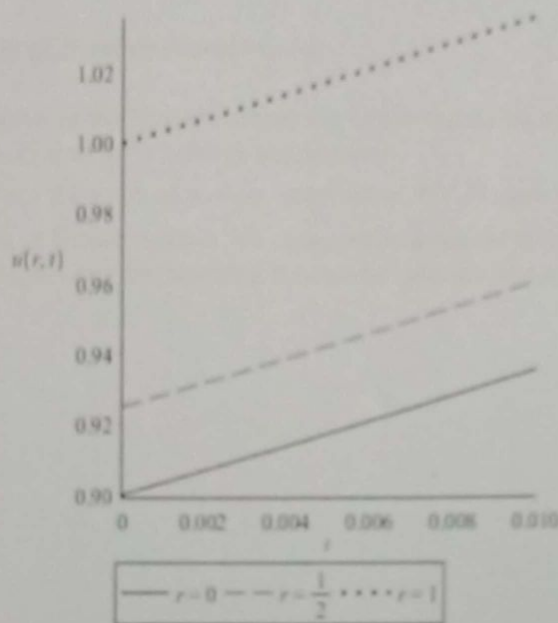A.W. Abubakar

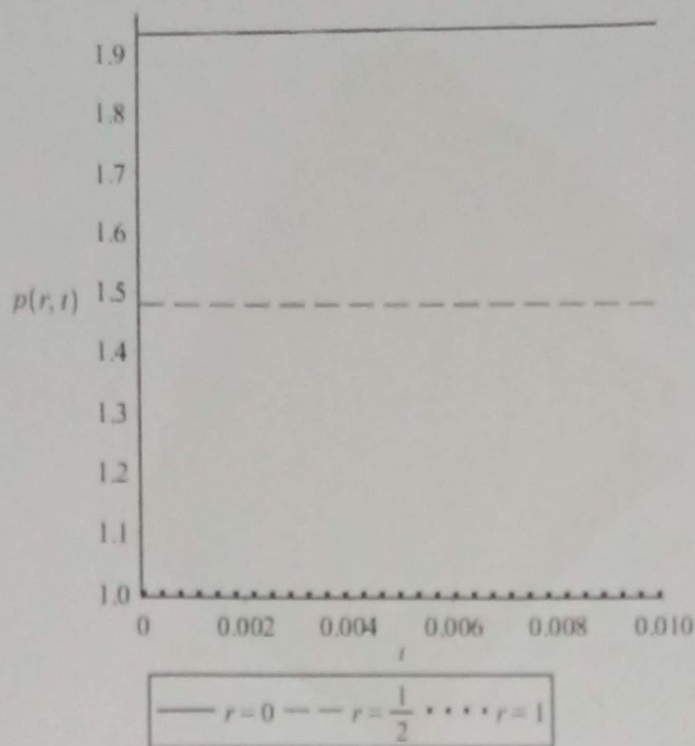Figure 3: Hydrocarbon Concentration

Figure 4: Droplet Velocity

Figure 5: Pressure

4.3   Effects of Nusselt Number, Nu

Numerical analysis of the Nusselt number was conducted to see whether or not the Nusselt number contribute significantly to the mixture temperature.

Figure 6 discloses the graph of mixture temperature $\theta(r,t)$ against time t and droplet radius r for different values of Nusselt number Nu. It is observed that the temperature of mixture increases with time and decreases along droplet radius but this temperature increases as Nusselt number increases.
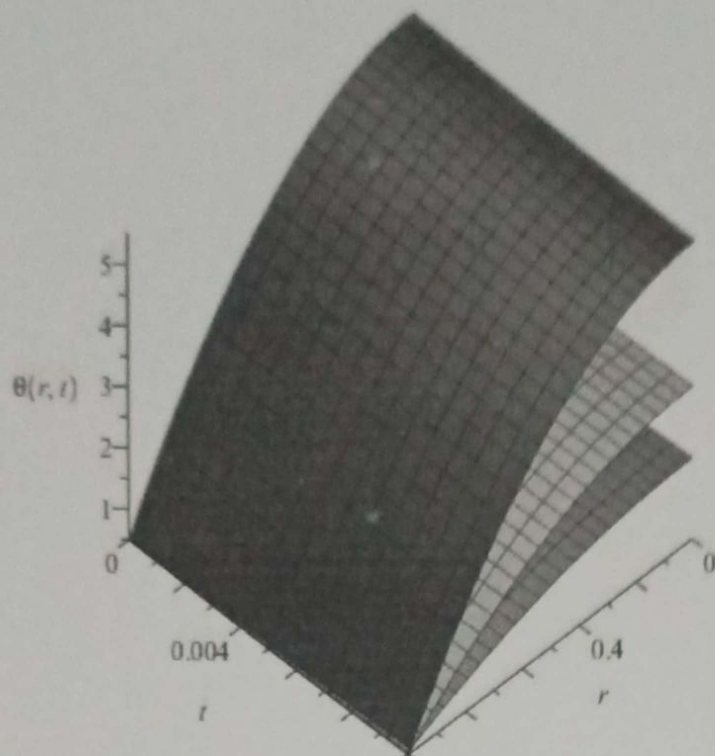
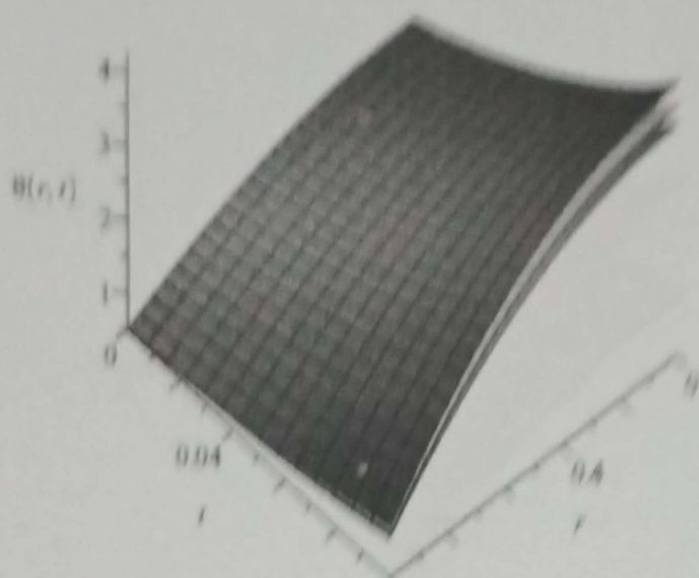**Figure 6:** Effects of Nusselt number, Nu on mixture temperature

4.4 Effects of Peclet Energy Number, P_e

Numerical analysis of the Peclet energy number was conducted to see whether or not the Peclet energy number contribute significantly to the mixture temperature.

Figure 7 depicts the graph of mixture temperature $\theta(r,t)$ against time t and droplet radius r for different values of Peclet energy number P_e. It is observed that the temperature of mixture increases with time and decreases along droplet radius but this temperature increases as Peclet energy number increases.
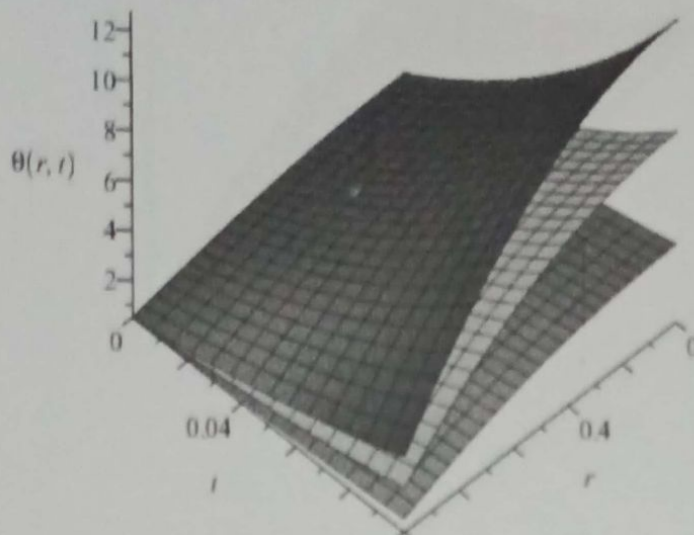
Figure 7: Effects of Peclet energy number, P_e on mixture temperature

4.5 Effects of Eckert Number, E_c

Numerical analysis of the Peclet energy number was conducted to see whether or not the Peclet energy number contribute significantly to the mixture temperature.

Figure 8 shows the graph of mixture temperature $\theta(r,t)$ against time t and droplet radius r for different values of Eckert number E_c. It is observed that the temperature of mixture increases with time and decreases along droplet radius but this temperature increases as Eckert number increases.

205
IJMAM, Vol. 5, Issue 2 (2022) CNSMB; www.tnsmb.org
(Formerly Journal of the Nigerian Society for Mathematical Biology)

Figure 8: Effects of Eckert number, E_c on mixture temperature

4.6 Effects of Darcy Number, D_a

Numerical analysis of the Darcy number was conducted to see whether or not the Darcy number contribute significantly to the mixture temperature, droplet velocity and pressure.

Figure 9 shows the graph of mixture temperature $\theta(r,t)$ against time t and droplet radius r for different values of Darcy number D_a. It is observed that the temperature of mixture increases with time and decreases along droplet radius but this temperature increases as Darcy number decreases.

Figure 10 displays the graph of droplet velocity $u(r,t)$ against time t and droplet radius r for different values of Darcy number D_a. It is observed that the velocity of droplet increases with time and increases along droplet radius but this velocity increases as Darcy number decreases. Figure 11 displays the graph of pressure $p(r,t)$ against time t and droplet radius r for different values of Darcy number D_a. It is observed that the pressure increases with time and decreases along droplet radius but this pressure increases as Darcy number decreases.
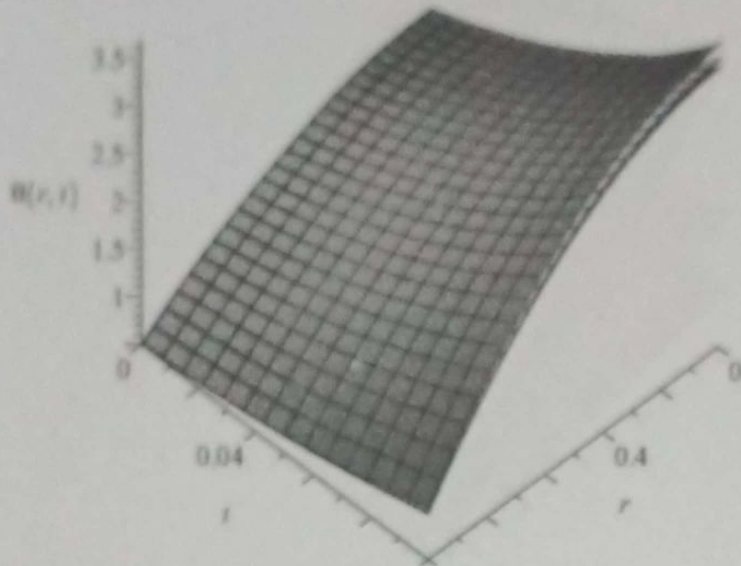
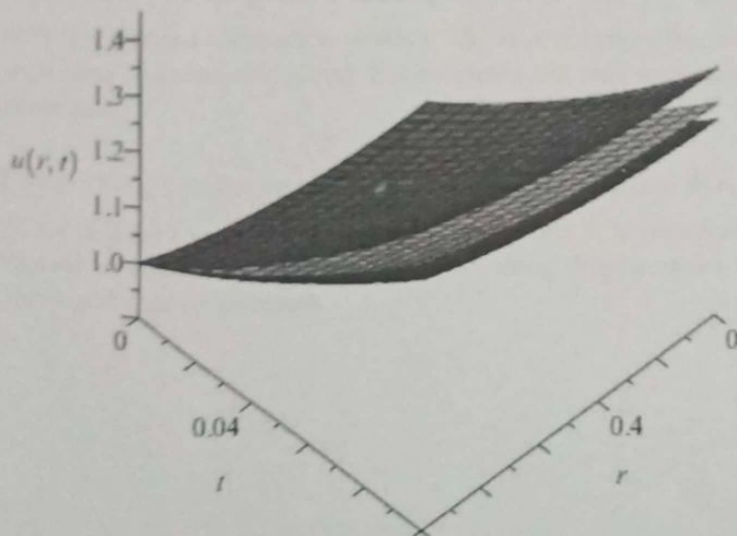**Figure 9**: Effects of Darcy number, D_a on mixture temperature

Figure 10: Effects of Darcy number, D_a on droplet velocity

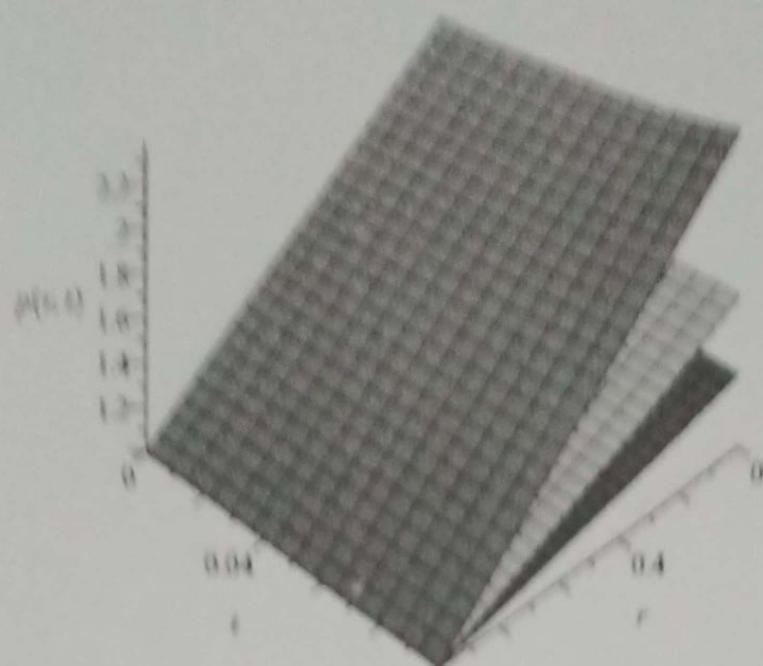R. O. Olayiwola, A. T. Cole, M. D. Shehu, F. A. Oguntolu, E. E. Iyeme, and
A. W. Abubakar

Figure 11: Effects of Darcy number, D_a on pressure

4.7 Effects of Sherwood Number, Sh

Numerical analysis of the Sherwood number was conducted to see whether or not the Sherwood number contribute significantly to the mixture temperature and carbon dioxide concentration.
Figure 12 shows the graph of mixture temperature $\theta(r,t)$ against time t and droplet radius r for different values of Sherwood number Sh. It is observed that the temperature of mixture increases with time and decreases along droplet radius but this temperature increases as Sherwood number decreases.

Figure 13 displays the graph of carbon dioxide concentration $\phi(r,t)$ against time t and droplet radius r for different values of Sherwood number Sh. It is observed that the concentration of carbon dioxide increases with time and decreases along droplet radius but this concentration increases as Sherwood number increases.
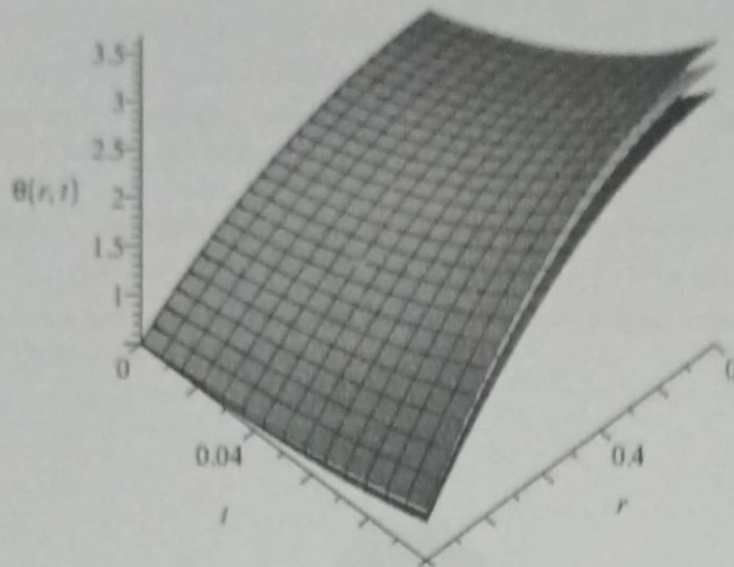
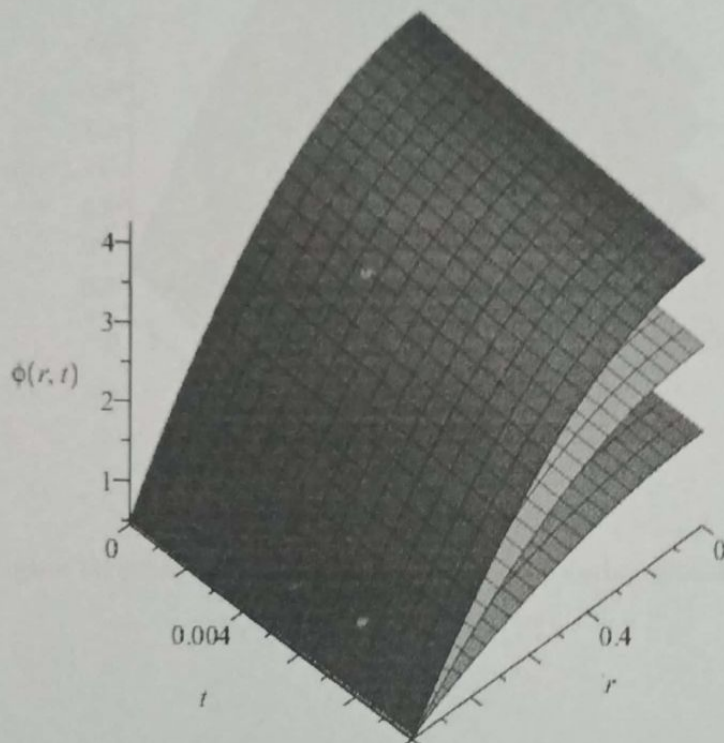**Figure 12**: Effects of Sherwood number, *Sh* on mixture temperature

Figure 13: Effects of Sherwood number, *Sh* on Carbon dioxide concentration

R.O. Olayiwola, A.T. Cole, M.D. Shehu, F.A. Oguntolu, E.E. Iyeme, and A.W. Abubakar

4.8 Effects of Peclet Mass Number, P_m

Numerical analysis of the Peclet mass number was conducted to see whether or not the Peclet mass number contribute significantly to the carbon dioxide and hydrocarbon concentrations.

Figure 14 shows the graph of carbon dioxide concentration $\phi(r,t)$ against time t and droplet radius r for different values of Peclet mass number P_m. It is observed that the concentration of carbon dioxide decreases with time and decreases along droplet radius but this concentration increases as Darcy number increases.

Figure 15 displays the graph of hydrocarbon concentration $\psi(r,t)$ against time t and droplet radius r for different values of Peclet mass number P_m. It is observed that the concentration of hydrocarbon increases with time and increases along droplet radius but this concentration increases as Darcy number decreases.
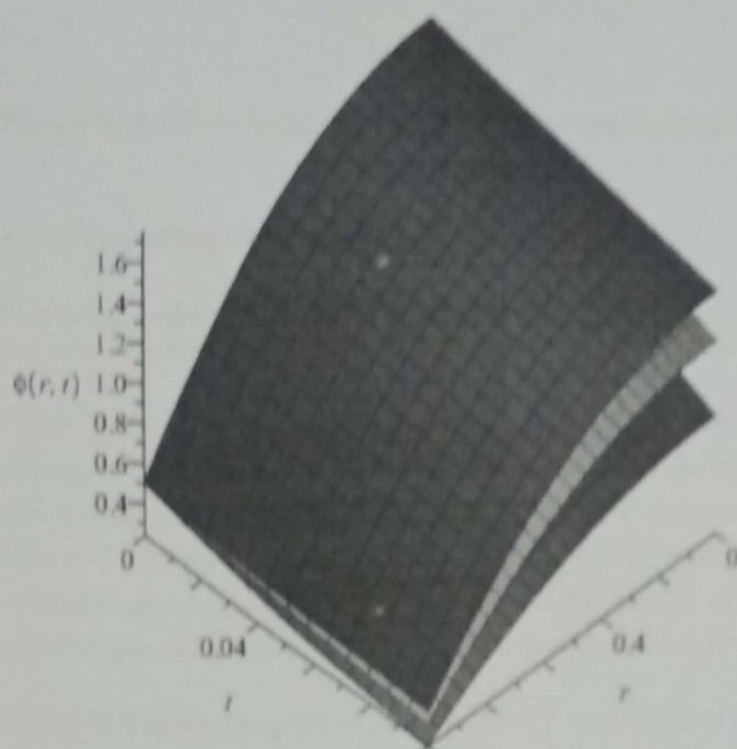

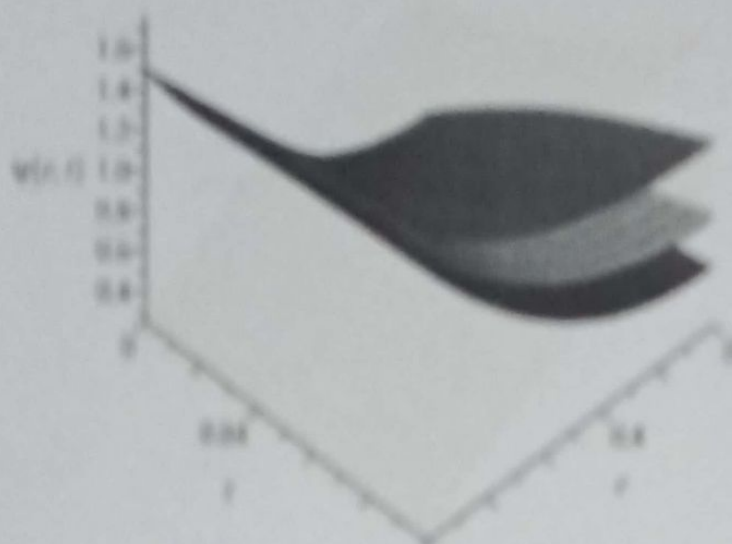**Figure 14:** Effects of Peclet mass number, P_m on Carbon dioxide concentration

Figure 18: Effects of Peclet mass number, P_{m} on hydrocarbon concentration

4.3 Effects of Reynolds Number, R_{e}

Numerical analysis of the Reynolds number was conducted to see whether or not the Reynolds number contributes significantly to the mixture temperature, droplet velocity and pressure.

Figure 16 shows the graph of mixture temperature $\theta(r,t)$ against time t and droplet radius r for different values of Reynolds number R_{e}. It is observed that the temperature of mixture increases with time and decreases along droplet radius but this temperature increases as Reynolds number decreases. Figure 17 displays the graph of droplet velocity $w(r,t)$ against time t and droplet radius r for different values of Reynolds number R_{e}. It is observed that the velocity of droplet increases with time and increases along droplet radius but this velocity increases as Reynolds number decreases.

Figure 18 displays the graph of pressure $p(r,t)$ against time t and droplet radius r for different values of Reynolds number R_{e}. It is observed that the pressure increases with time and decreases along droplet radius but this pressure increases as Reynolds number decreases.
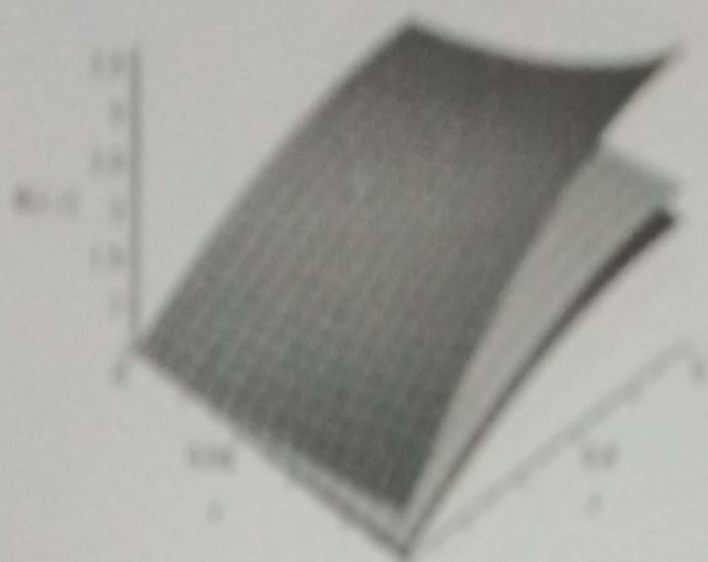
K.O. Olayiwola, A.T. Cole, M.D. Shehu, F.A. Oguntolu, E.E. Ayoma, and A.W. Abubakar

Figure 36 Effects of Reynolds number, R_e on nutrient temperature
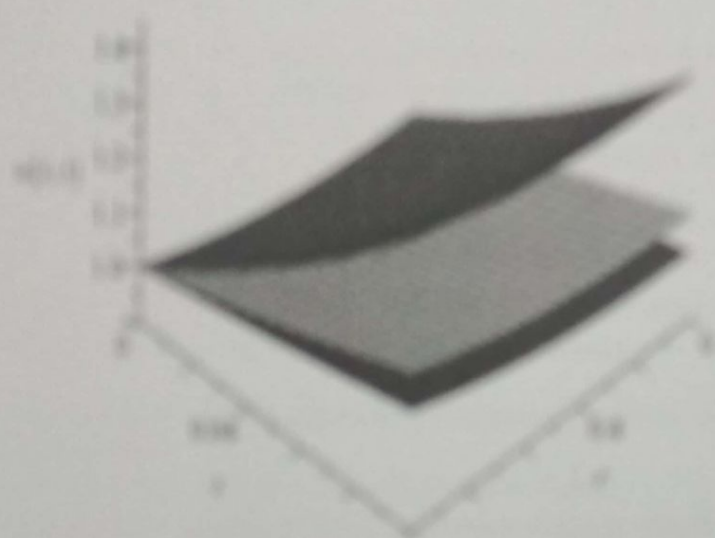
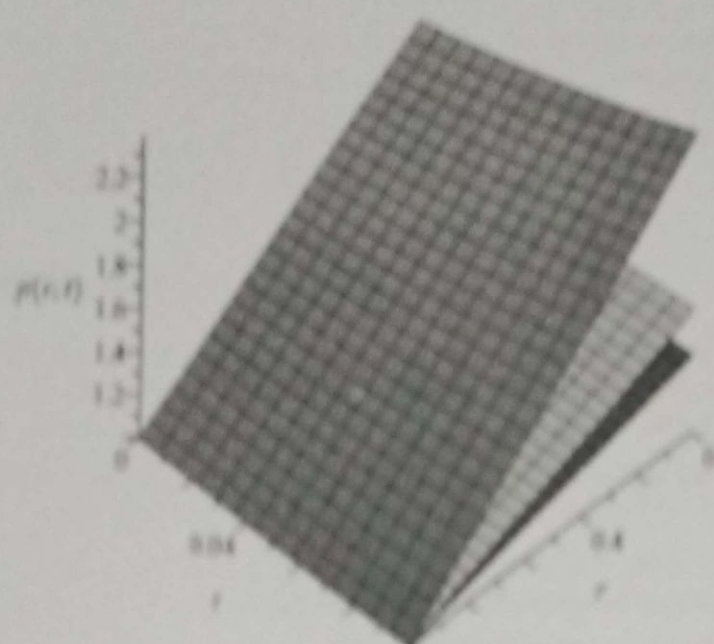**Figure 37** Effects of Reynolds number, R_e on angular velocity

Figure 18: Effects of Reynolds number, R_e on pressure

It is worth pointing out that the effects observed in Figures 1 to 18, are important for designing and optimising different CO_2 antisolvent processes for the formulation of small crystalline drug products.

5 Conclusion

This research work developed a model describing heat and mass transfer between a droplet of solvent (hydrocarbon) and a compressed antisolvent (carbon dioxide) in miscible conditions taking into consideration the viscous energy dissipation and transfer of heat and mass between the reservoir surface and the droplet by convection, in order to investigate the role of operating parameters on droplet lifetime. This model which relies on several assumptions is based on the conservation of total mass, chemical species, momentum and energy written in transient state mode of operation. The governing parameters of the problem are the Eckert number (E_c), Peclet energy number (P_e), Reynolds number (R_e), Peclet mass number (P_m), Darcy number (D_a), Nusselt number (Nu) and Sherwood number (Sh). The study revealed the following:

The mixture temperature, hydrocarbon concentration, pressure and velocity of droplet are increasing functions of time.

The CO_2 concentration is a decreasing function of time.

The mixture temperature is higher at the centre of droplet than at the end of domain.

There is higher concentration of CO_2 at the centre of droplet than at the end of domain.

There is higher concentration of hydrocarbon at the end of domain than at the centre of droplet.

R.O. Olayiwola, A.T. Cole, M.D. Shehu, F.A. Oguntolu, E.E. Iyeme, and A.W. Abubakar

The velocity of droplet is higher at the end of domain than at the centre of droplet.
The pressure is higher at the end of domain than at the centre of droplet.

The results highlighted above showed that the particle formation in drug production could be controlled by the governing parameters involved. These results are useful in pharmaceutical industries for achieving very small drug particles of interest. The results of this study may be of importance to engineers and scholars attempting to develop programming standards and to researchers interested in the theoretical aspects of computer programming.

References

[1] Almeida R.A., Rezende R.V.P., Guirardello R., Meier H.F., Noriler D., Filho L.C., and Cabral V. F. (2015). Numerical study of the impact of the solution flow rate in the supercritical antisolvent process: a 3D approach. Chemical Engineering Transactions, Vol. 43: 1633 – 1638.

[2] Beckman E.J. (2004). Supercritical and near critical CO2 in green chemical synthesis and processing. Journal of Supercritical Fluids, Vol. 28(2-3): 121 - 191.

[3] Bristow S., Shekunov T., Shekunov B.Y., and York P. (2001). Analysis of the supersaturation and precipitation process with supercritical CO2. Journal of Supercritical Fluids, Vol. 21: 257 - 271.

[4] Chang A. A. (2006). Study of particle formation using supercritical CO2 as an antisolvent. A PhD Thesis, North Carolina State University, Raleigh, North Carolina.

[5] Chong G. H., Spotar S.Y., and Yunus R. (2009). Numerical modelling of mass transfer for solvent-Carbon Dioxide system at supercritical (miscible) conditions. Journal of Applied Sciences, Vol. 9(17): 3055 – 3061.

[6] Hughes W.F. and Gaylord E W. (1964). Basic equations of engineering science. Schaum's Outline Series, McGraw-Hill Book Company, New York.

[7] Jung J. and Perrut M. (2001). Particle design using supercritical fluids: Literature and patent survey. Journal of Supercritical Fluids, Vol. 20: 179 - 219.

[8] Keshavarz P. and Taheri M. (2007). An improved lumped analysis for transient heat conduction by using the polynomial approximation method. Heat Mass Transfer, Vol. 43: 1151 – 1156.

[9] Kumar R., Mahalingam H. and Tiwari K. (2012). Modeling of droplet composition in supercritical antisolvent process: Part A. International journal of Chemical Engineering and Application, Vol. 3(6): 456 – 460.

[10] Louey M.D., Van Oort M. and Hickey A.J. (2004). Aerosol dispersion of respirable particles in narrow size distributions produced by jet-milling and spray drying techniques. Pharmaceutical Research, Vol. 21(7): 1200 - 1206.

[11] McHugh M.A. and Krukonis V.J. (1994). Supercritical fluid extraction. 2nd ed. Newton, MA: Butterworth-Heinemann.

[12] Mujumdar A.S. (1987). Handbook of Industrial Drying. Marcel Dekker, Inc. 295-323.

[13] Olayiwola R.O. (2015). Modeling and simulation of combustion fronts in porous media. Journal of Nigeria Mathematical Society, Vol. 2 (1): 100 – 103.

[14] Padreis L., Rodrigues M. A., Velaga S.P., Matos H.A., Azevedo E.G. (2009). Formation of indomethacin-saccharin co-crystals using supercritical fluid technology. European Journal of Pharmaceutical Sciences, Vol. 38 (1): 9 – 17.

[15] Prakash A. and Mahmood S. (2013). Modified lumped model for transient heat conduction in spherical shape. American International Journal of Research in Science, Technology, Engineering & Mathematics, Vol. 2(2): 155 – 159.

[16] Reverchon E. and Della Porta G. (2001). Supercritical fluids assisted micronization techniques. Low impact route for particle production. Pure and Applied Chemistry, Vol. 73(8): 1293 - 1297.

[17] Rogers T.L., Johston K.P. and Williams R.O. (2001). Solution based particle formation of pharmaceutical powders by supercritical or compressed fluid CO2 and cryogenic spray freezing technologies. Drug Development and Industrial Pharmacy, Vol. 27(10): 1003 - 1015.

[18] van de Weert M., Hennink W.E., and Jiskoot W. (2000). Protein instability in poly (Lactic-co-Glycolic Acid) microparticles. Pharmaceutical Research, Vol. 17(10): 1159 - 1167.

[19] Wu G., Dabiri S., Timko M.T., and Ghoniem A.F. (2012). Fractionation of multi-component hydrocarbon droplets in water at supercritical or near-critical conditions. Journal of Supercritical Fluids, Vol. 72: 150 – 160.